

Article

Wear Prediction of Curved Switch Rail in High-Speed Turnout and Influence of Wheel and Rail Wear on Vehicle Dynamic Performance

Shuo Yan ¹, Taotao Jin ^{1,2,3,*}, He Ma ¹, Jun Zhang ^{1,2,3,*} and Yi Zhou ¹

- ¹ School of Mechanical–Electronic and Vehicle Engineering, Beijing University of Civil Engineering and Architecture, Beijing 100044, China; 2108550021126@stu.bucea.edu.cn (S.Y.); mahe@bucea.edu.cn (H.M.); 2108550022069@stu.bucea.edu.cn (Y.Z.)
- ² Beijing Key Laboratory of Performance Guarantee on Urban Rail Transit Vehicles, Beijing 100044, China
- ³ Beijing Engineering Research Center of Monitoring for Construction Safety, Beijing 100044, China
- * Correspondence: jintao@bucea.edu.cn (T.J.); zhangjun611@bucea.edu.cn (J.Z.);
Tel.: +86-15801599683 (T.J.); +86-13611277353 (J.Z.)

Abstract: A wear prediction model is built to research the wear of the curved switch rail in a high-speed turnout. The Archard wear model is used in the wear prediction model to analyze the profile evolution law. The non-Hertzian contact Kik–Piotrowski method based on virtual penetration is used as the contact algorithm for the Archard wear model. A dynamic model of the vehicle–curved switch rail system based on the predicted profiles of the curved switch rail and the measured wheel profiles with different stages is established. The effect of the wheel and curved switch rail profiles' wear on vehicle dynamic performance is analyzed. The results show that the wheel completely transitions from the stock rail to the curved switch rail between 35 and 50 mm head widths. As the head width of the curved switch rail increased, the position of the maximum wear depth gradually moved to the gauge shoulder. When the total passing weight of the train is 50 Mt, the 20 mm head width curved switch rail side wear reaches a maximum of 5.3 mm. The position in which the wheel transitions from the stock rail to the curved switch rail will be further away from the tip of the curved switch rail due to wheel–rail wear. Regarding the derailment coefficient, the wheel–rail vertical force and lateral force are both significantly impacted. However, they have little effect on the vertical and lateral acceleration of the vehicle. The wear of the wheels and rails has a higher impact on vehicle driving safety and a lower impact on vehicle driving stability.

Keywords: high-speed turnout; curved switch rail; wear prediction; dynamic performance



Citation: Yan, S.; Jin, T.; Ma, H.; Zhang, J.; Zhou, Y. Wear Prediction of Curved Switch Rail in High-Speed Turnout and Influence of Wheel and Rail Wear on Vehicle Dynamic Performance. *Appl. Sci.* **2023**, *13*, 8398. <https://doi.org/10.3390/app13148398>

Academic Editor: Sakdirat Kaewunruen

Received: 26 May 2023
Revised: 14 July 2023
Accepted: 15 July 2023
Published: 20 July 2023



Copyright: © 2023 by the authors. Licensee MDPI, Basel, Switzerland. This article is an open access article distributed under the terms and conditions of the Creative Commons Attribution (CC BY) license (<https://creativecommons.org/licenses/by/4.0/>).

1. Introduction

Turnout is a track component that enables trains to change from one track to another and plays an essential role in the railway system. It is also the weakest link of the track. As a result, turnout components are more prone to failure compared with a typical rail piece [1]. The turnout consists of three parts: switch, closure, and crossing panels [2]. In the switch panel, the direction of the vehicle can be changed by moving its wheels between the stock rail and the switch rail [3]. In this process, the wheel–rail relationship is more complex. The curved switch rail is a variable section structure that is highly susceptible to damage when subjected to complex loads.

Many scholars have researched wheel–rail wear and wear prediction. Authors [4–7] conducted tracking tests on the wear state of the wheels of vehicles running on a line, and dynamic models of the vehicle were implemented to analyze the effect of wheel wear on dynamic performance. Jin et al. [8] carried out a detailed analysis and summarized the transverse wear of China's high-speed wheel and rail and proposed seven measures to suppress or slow down the concave wear near the nominal rolling circle of the wheel. The

influence of out-of-round railway wheels on the dynamic characteristics of the wheel–rail systems were studied by the authors of [9–11]. Wang et al. [12] explored the variability of rail wear on heavy-haul railways under different conditions.

Kaewunruen et al. [13–17] studied the railway system from multiple perspectives. They proposed a new hybrid numerical–analytical method for predicting the vertical leveling loss of railway track geometry under dynamic cyclic loadings, comprehensively considering operational, vehicle, and track conditions [13]. The train–track–soil interaction model was established to analyze the dynamic wheel–rail interaction under track irregularities [14]. The effects of conditions such as floods, crosswinds, and moving train loads on the track were also considered [15–17]. In addition, Pradhan et al. [18] performed wear calculations for vehicles running on a route in India and made recommendations. A calculation method based on finite element friction work was suggested by Wang et al. [19] to predict wheel tread wear. Furthermore, the wear evolution of curved rails was computed by Wu et al. [20], and the vertical and lateral wear rates of the railway with 60 and 60 N profiles were compared. Ma et al. [21] built a curved rail side wear prediction model and summarized the wear law of the Shuohuang heavy-haul railway. To analyze the influence of hollow-worn wheels on rail wear, Sun et al. [22,23] proposed a numerical model for the prediction of non-uniform wear on rails. The non-uniform wear evolution of rails and its effect on the dynamic wheel–rail interaction was investigated. Li et al. [24] used the Hertz–FASTRIP–USFD model for rail wear calculation to predict the development law of rail wear on curve sections of urban rail transit lines.

The wheel–rail contact state in the turnout is more complicated, and many scholars have researched the wheel–rail contact relationship in this area. Gao et al. [25] compared and analyzed the wear effects of 60 and 60 N profiles on straight and curved switch rails. Wang et al. [26,27] investigated the effect of the friction coefficient between wheel and rail on the wear of curved switch rails when a vehicle passes a turnout in the branch direction. Zhang [28] analyzed the influence of different side wear degrees of switch rails on wheel–rail dynamics. In order to study the effect of impact loads on train–turnout systems, Hamarat et al. [29,30] developed a finite element model that captures the impact and dynamic forces due to track irregularities and is validated by field measurements. Nielsen et al. [31] proposed a method to simulate the vertical dynamic interaction between a wheelset and railway track; wheel–rail impact loads and axle stresses were computed for different distributions. Based on Bayesian networks, Dindar et al. [32,33] analyzed the influence of human error and climatic factors on railway turnout systems, providing an integrated approach to dealing with the many different risks arising from a variety of sources in the railway turnout system.

Multi-point wheel–rail contacts are more common in turnouts do not satisfy the basic assumptions of Hertzian theory. The non-Hertz contact theory can more realistically reflect the state of wheel–rail interactions. Yang et al. [34,35] used a non-Hertzian contact method to analyze the dynamic wheel–rail interaction characteristics for gauging corner lubrication and changeable friction conditions. Carlberger et al. [36] proposed a versatile numerical method for predicting the long-term growth of rail roughness—a post-calculation of sliding wear based on Archard’s wear model in combination with a non-Hertzian and transient wheel–rail contact model was used. To improve computational efficiency, many scholars have proposed a series of non-Hertzian contact simplification algorithms based on virtual penetration theory, such as the Kik–Piotrowski method [37,38], ANALYN method [39], and so on. Wang et al. [40,41] compared the accuracy and efficiency of several algorithms and the Kik–Piotrowski method considers both computational accuracy and efficiency. Lin et al. [42], in combination with the wheel–rail contact algorithm of a non-elliptical multi-point contact Kik–Piotrowski model, calculated the wheel–rail dynamic variation characteristics and wheel–rail wear characteristics of worn wheels passing through the frog area under different friction coefficients. Based on the Kik–Piotrowski method, Fan et al. [43] established the turnout model with variable cross-section and multi-point contact and analyzed the dynamic response of the train passing through the branch

of the turnout. Wang [44,45] carried out the calculation of wear distribution for a No. 42 turnout curved switch rail and stock rail and summarized the rail's wear law. The rails in the field were also measured, and the measured data provided experimental validation for the wear simulation.

Most of the existing wear prediction methods use the Archard wear model to predict wear on the wheel–rail profile, while wear predictions for the curved switch rail, which is a variable section, have rarely been reported. In this study, the wheel profiles were tracked and measured. The key sections of the curved switch rail of a No. 18 turnout are drawn and discretized into nodes, which are then imported into Universal Mechanism software. The non-Hertzian contact Kik–Piotrowski method based on virtual penetration is used as the contact algorithm for the Archard wear model. The worn profiles of the curved switch rail are predicted, and the wear evolution law is analyzed. Based on the predicted calculation results of the curved switch rail wear and the actual measured wheel profiles, simulations are performed in a vehicle–curved switch rail system dynamics model. The effect of the wear of the wheel and curved switch rail on vehicle dynamic performance is analyzed.

2. System Dynamics Model of Vehicle–Curved Switch Rail

2.1. Establishment of Curved Switch Rail Model in High-Speed Turnout

The radius of the curved switch rail equals 1100 m in the No. 18 high-speed turnout. In the switch panel, the switch rail adopts the 60D40 steel track, and the stock rail adopts the 60 kg/m steel track. The gauge is 1435 mm. The vertical stiffness of the track is 44,000 kN/m, and the lateral stiffness is 18,000 kN/m. The vertical and lateral damping are 400,000 Ns/m and 100,000 Ns/m, respectively.

The curved switch rail is a variable section structure, and the cross-section and head width gradually increase. According to the head width size of the curved switch rail, the profiles with head widths of 3 mm, 5 mm, 20 mm, 35 mm, 50 mm, and 72.2 mm are selected for modeling (Figure 1).

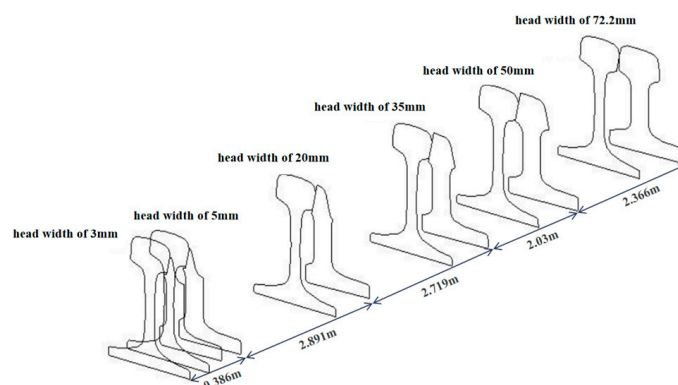


Figure 1. Key sections of curved switch rail in high-speed turnout.

In the switch panel, the cross-sections of the switch rail and are variable. To establish the system dynamic model of the vehicle and curved switch rail, the transition of each adjacent irregular critical section is performed by the interpolation method. In this way, the entire curved switch rail model is fitted. Figure 2 illustrates the cross-sectional interpolation principle.

2.2. Vehicle Dynamic Model

A non-contact infrared wheel track profile measuring instrument is used to track the wheel profiles. According to the side wear depth, the worn wheels are divided into four wear stages and defined as wear type I profile, wear type II profile, wear type III profile, and wear type IV profile. The standard xp55 profile and worn profiles are shown in Figure 3.

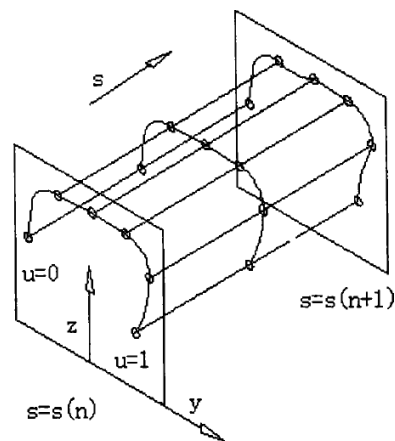


Figure 2. Principle of cross-sectional interpolation.

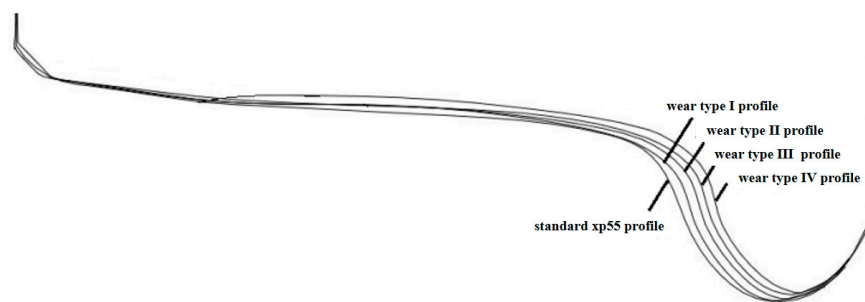


Figure 3. Wheel profiles of the standard and different wear stages.

Table 1 shows the side wear values of wheel flanges in different wear stages. More serious wear is present on the wheel flange and in the middle of the tread. With the wear aggravation of the wheel, the side wear of wheel flange gradually deepened. For the standard xp55, wear type I, wear type II, wear type III, and wear type IV profiles, the wheel flange side wear values for the five types of wheel profiles are 0, 1.743, 3.432, 4.719, and 6.208 mm, respectively. The wear type IV profile wheels have the greatest depth of side wear at 6.208 mm. Compared with the standard xp55 wheel profile, the flange side wear depth of the wear type I wheel profile increases by 1.743 mm, the increase is the largest among the four wear stages.

Table 1. Side wear values of wheel flange with different wear stages.

Wear Stages	Side Wear Values/mm
standard xp55 profile	0
wear type I profile	1.743
wear type II profile	3.432
wear type III profile	4.719
wear type IV profile	6.208

Side wear will lead to the thinning of the train wheel flange, which is one of the typical forms of wheel damage. In addition, it affects the safety of train operations. The limit value of wheel flange thickness in China is 22 mm. When the wheel flange thickness is less than 22 mm, it is necessary to repair it.

The UM software is applied to build the vehicle model of the CRH5 EMU (electric multiple unit), as shown in Figure 4. The vehicle model is made up of one car body and two bogies. The main parts, such as the car body, bogie, wheelset, and axle box, are rigid solid bodies without simplification. The suspension components include the primary spring, primary vertical damper, secondary air spring, secondary longitudinal damper

(anti-serpentine shock absorber), and secondary lateral damper. Part parameters of CRH5 EMU are shown in Table 2.

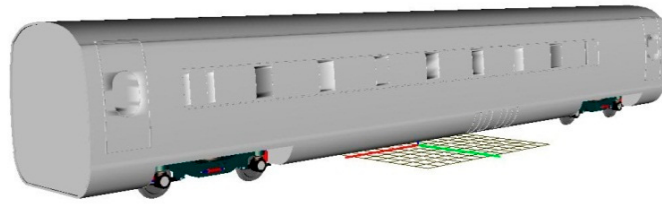


Figure 4. Multibody dynamics model of CRH5.

Table 2. Part parameters of CRH5 EMU.

Parameters	Value
Car body mass (kg)	41,190
Car body rolling moment of inertia ($\text{kg}\cdot\text{m}^2$)	79,600
Car body pitching moment of inertia ($\text{kg}\cdot\text{m}^2$)	2,105,000
Car body yawing moment of inertia ($\text{kg}\cdot\text{m}^2$)	2,093,000
Bogie frame mass (kg)	2920
Bogie frame rolling moment of inertia ($\text{kg}\cdot\text{m}^2$)	2247
Bogie frame pitching moment of inertia ($\text{kg}\cdot\text{m}^2$)	2860
Bogie frame yawing moment of inertia ($\text{kg}\cdot\text{m}^2$)	5040
Wheelset mass (kg)	1523
Wheelset rolling moment of inertia ($\text{kg}\cdot\text{m}^2$)	708
Wheelset pitching moment of inertia ($\text{kg}\cdot\text{m}^2$)	100
Wheelset yawing moment of inertia ($\text{kg}\cdot\text{m}^2$)	708
Vertical stiffness of primary spring (N/m)	1,500,000
Longitudinal stiffness of primary spring (N/m)	980,000
Lateral stiffness of primary spring (N/m)	980,000
Vertical damping of primary vertical shock absorber (N·s/m)	10,000
Vertical stiffness of secondary suspension (N/m)	450,000
Longitudinal stiffness of secondary spring (N/m)	20,0000
Lateral stiffness of secondary spring (N/m)	200,000
Vertical damping of secondary vertical shock absorber (N·s/m)	20,000
Longitudinal damping of secondary longitudinal shock absorber (N·s/m)	360,000
Lateral damping of secondary lateral shock absorber (N·s/m)	22,000

The evaluation indices for the safety and stability of high-speed EMU operation mainly include the wheel–rail vertical and lateral force, derailment coefficient, and vertical and lateral acceleration. In order to ensure the safe and stable operation of vehicles, the above-mentioned indicators are limited to a “Specification for Dynamic Performance Assessment and Test Verification of Rolling Stock” (GB/T 5599–2019), which is shown in Table 3.

Table 3. The limit of each dynamic index of CRH5.

Dynamic Index	Specified Limit Value
Wheel–rail vertical force	≤ 170 kN
Wheel–rail lateral force	≤ 48.4 kN
Derailment coefficient	< 0.8
Vertical acceleration	< 2.5 m/s ²
Lateral acceleration	< 2.5 m/s ²

2.3. Vehicle and Curved Switch Rail System Dynamics Model

The vehicle and curved switch rail are connected by the wheel–rail relationship. As shown in Figure 5, the dynamic model of the vehicle–curved switch rail system has been established.

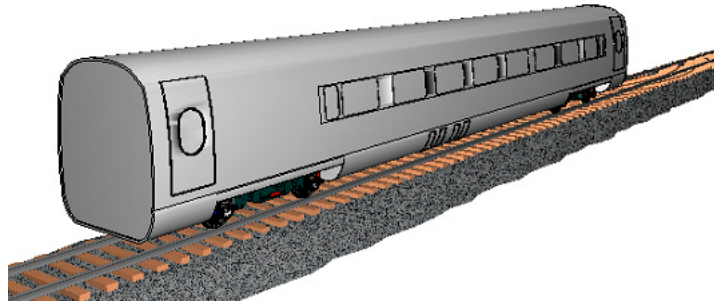


Figure 5. The system dynamics model of the vehicle and curved switch rail.

The curved switch rail has a variable section structure. Multiple contact modes occur between the wheels and rails when the vehicle passes through this area. The hypothetical conditions of the traditional Hertz theory are idealized. The calculation of the multi-point contact relationship between the wheels and rails will have errors, and the calculation results will be quite different from the actual situation [46]. The Kalker non-Hertzian contact theory, which takes into account the actual wheel–rail contact shape, can be used to compute the precise solution of three-dimensional rolling contact. However, the rate of calculation is rather slow [37]. The Kik–Piotrowski method solves the problem of slow calculation speed and ensures the accuracy and efficiency of calculation. The Universal Mechanism uses the non-Hertzian contact Kik–Piotrowski method based on virtual penetration as a contact algorithm for the Archard wear model. It predicts realistic wheel–rail profiles and takes into account the efficiency of the calculation. Therefore, this paper uses it to predict the wear on key sections of curved switch rails.

2.4. Kik–Piotrowski Contact Theory and Archard Wear Model

In the case of complex wheel–rail contact in the turnout area, the shape of the contact area between the wheels and rails being an ellipse cannot better reflect the actual situation. The normal stress distribution of the wheel and rail during rolling is assumed to be semi-elliptical by Kik and Piotrowski, and the contact area is confirmed by using the virtual penetration method [37,38].

The virtual penetration region between the wheel and rail is determined by the depth of penetration δ_0 , which is taken as the contact area. The penetration function $g(y)$ is expressed in Equation (1):

$$g(y) = \begin{cases} \delta_0 - f(y) & f(y) \leq \delta_0 \\ 0 & f(y) > \delta_0 \end{cases} \tag{1}$$

where $f(y)$ is the distance in the rolling direction between the rail and wheel at the same coordinate.

In the penetration area, the x coordinates of the front and rear ends are:

$$x_l(y) = -x_r(y) \approx \sqrt{2Rg(y)} \tag{2}$$

where R is the wheel rolling circle radius.

The distribution of normal contact stress p in the contact patch is shown in Equation (3):

$$p(x, y) = \frac{p_0}{x_l(0)} \sqrt{x_l^2(y) - x^2} \tag{3}$$

where p_0 is the maximum normal contact stress in the contact patch.

Integrating the above equation yields the total normal force of the contact patch N .

$$N = \frac{p_0}{x_l(0)} \left(\int_{y_r}^{y_l} \int_{-x_l}^{x_l} \sqrt{x_l^2(y) - x^2} dx dy \right) \tag{4}$$

Using the Boussinesq function, the normal displacement at the point (0,0) is calculated using Equation (5):

$$\frac{\delta_0}{2} = \omega_0 = \frac{1 - \sigma_0}{\pi E} \frac{p_0}{x_l(0)} \left(\int_{y_r}^{y_l} \int_{-x_l}^{x_l} \frac{\sqrt{x_l^2(y) - x^2}}{\sqrt{x^2 + y^2}} dx dy \right) \quad (5)$$

Through the above two equations, the calculation of normal force and maximum contact stress are obtained, as shown in Equations (6) and (7):

$$N = \frac{\pi E \delta}{2(1 - \sigma^2)} \left(\int_{y_r}^{y_l} \int_{-x_l}^{x_l} \frac{\sqrt{x_l^2(y) - x^2}}{\sqrt{x^2 + y^2}} dx dy \right)^{-1} \left(\int_{y_r}^{y_l} \int_{-x_l}^{x_l} \sqrt{x_l^2(y) - x^2} dx dy \right) \quad (6)$$

$$p_0 = N \sqrt{2R\delta_0} \left(\int_{y_r}^{y_l} \int_{-x_l}^{x_l} \sqrt{x_l^2(y) - x^2} dx dy \right)^{-1} \quad (7)$$

The Archard model is one of the most important wear prediction models in the field of wheel–rail wear research. In the model, the wear volume is proportional to the normal force and sliding distance between the two contact bodies and inversely proportional to the material hardness [47], as shown in Equation (8):

$$V = k \frac{NS}{H} \quad (8)$$

where V is the wear volume, N is the normal force between the wheel and rail, S is the relative sliding distance, H is the material hardness, and k is the wear coefficient.

The sliding distance between wheel and rail is calculated using Equation (9). The relative sliding speed of wheel and rail is calculated using Equation (10):

$$S = |v_s| \frac{\Delta x}{v_0} \quad (9)$$

$$v_s = v_0 \left[\begin{matrix} \zeta - x_2 \phi - \frac{\partial u_1}{\partial x_1} \\ \eta + x_1 \phi - \frac{\partial u_2}{\partial x_1} \end{matrix} \right] \quad (10)$$

where v_s is the relative sliding speed of wheel and rail, v_0 is the wheel rolling speed, and u_1 , u_2 are the elastic displacements of the particles along the longitudinal and lateral directions, respectively. ζ , η , and ϕ are the longitudinal, lateral, and spin creepage values within the wheel–rail contact patch, respectively.

Jendel [48] obtained the relationship between wear coefficient, contact stress, and sliding velocity by summarizing the results of wheel–rail wear tests, as shown in Figure 6.

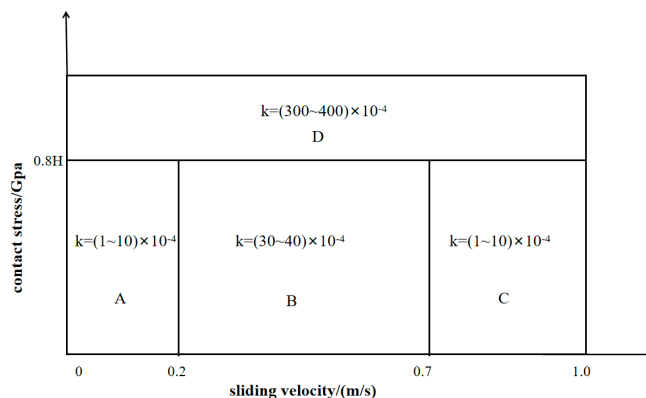


Figure 6. Wear coefficient distribution.

3. Wear Prediction of Curved Switch Rail

3.1. Wear Prediction Model of Curved Switch Rail

The flow chart of the curved switch rail profile prediction is shown in Figure 7. The vehicle–curved switch rail dynamics model is used to perform dynamics simulation calculations and obtain wheel–rail contact parameters. The non-Hertzian contact Kik–Piotrowski method based on virtual penetration is used as a contact algorithm. The wear depth of each unit in the contact patch is calculated using the Archard wear model, and they are added to obtain the wear depth of the entire contact patch. The wear of each contact patch is accumulated on the curved switch rail profile using a cubic spline interpolation approach.

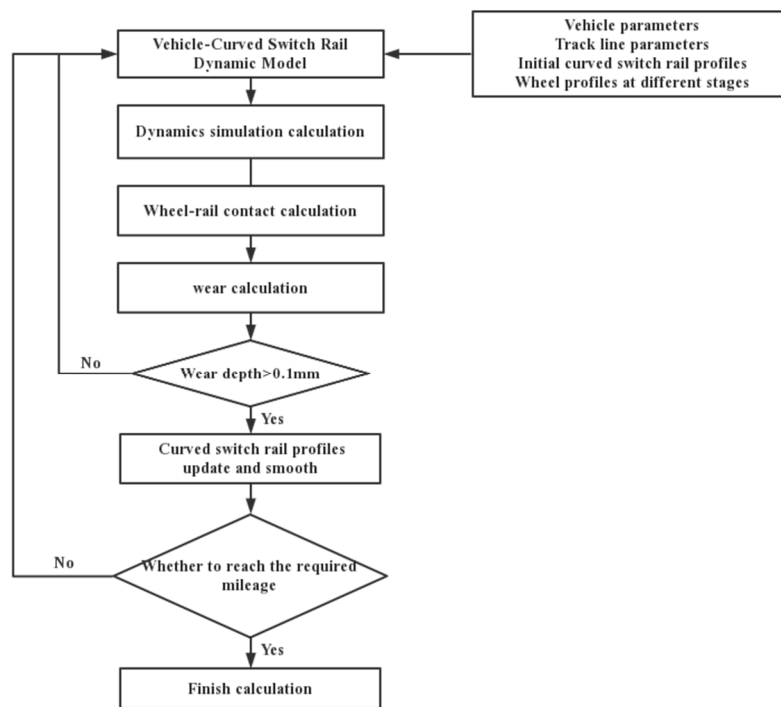


Figure 7. Flow chart of wear prediction of curved switch rail.

The profile will be updated and smoothed when the wear depth in the curved switch rail profile reaches 0.1 mm. Otherwise, the wear depth calculation continues. The new curved switch rail profile is obtained by subtracting the wear depth from the initial profile. If the specified mileage is not reached, the new curved switch rail profile will enter the next cycle. Once the specified mileage is reached, the calculation ends, and the predicted profile is output.

The variations in the curved switch rail profile and the vehicle–curved switch rail system dynamics are mutually influenced. As vehicle mileage increases, the curved switch rail will continue to wear out. The dynamic response and wheel–rail contact state will affect the prediction of the curved switch profile. The change in profile will in turn affect the dynamic response and wheel–rail contact state.

3.2. Profile Prediction of Curved Switch Rail

As shown in Figure 8, the worn profiles of the curved switch rail in the key sections for the total passing weights of 10 Mt, 20 Mt, 30 Mt, 40 Mt, and 50 Mt are calculated according to the methodology presented in Section 3.1.

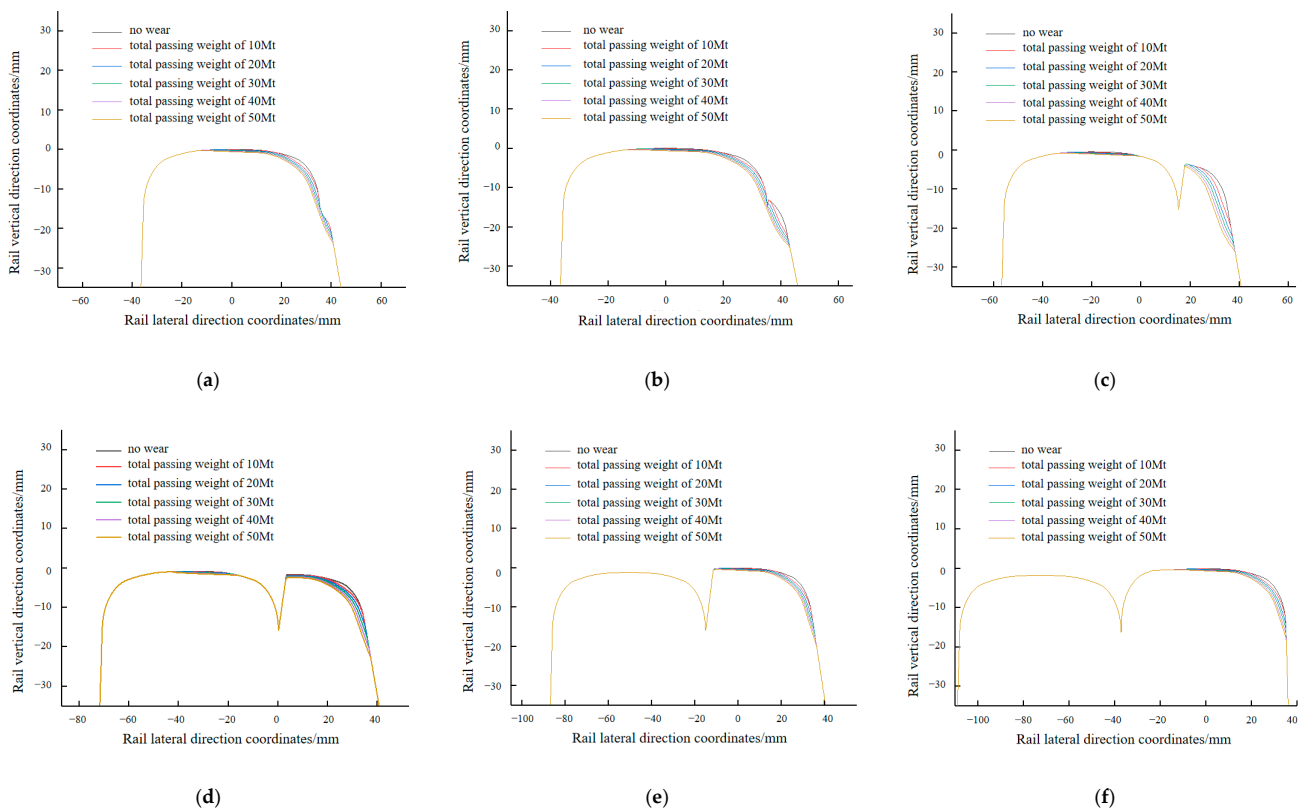


Figure 8. Comparison of a profile of key sections of worn curved switch rail: (a) head width 3 mm; (b) head width 5 mm; (c) head width 20 mm; (d) head width 35 mm; (e) head width 50 mm; (f) head width 72.2 mm.

The wheels make simultaneous contact with the stock rail and curved switch rail when the vehicle passes over the curved switch rail with a head width of 3 mm to 35 mm. The curved switch rail height will exceed the stock rail with the increase in head width, and the wheels will travel from the stock rail to the curved switch rail. The wear of the stock rail at the head width of 3 mm section is serious. As the head width increases, the wear depth of the stock rail decreases, while the wear depth of the curved switch rail rises. The wheels are completely transitioned from the stock rail to the curved switch rail in the 35–50 mm head width area. The wear depth of the curved switch rail is significantly reduced when the transition is complete. The contact position of the rail head gradually moves to the rail side as it passes through the 50–72.2 mm head width area. With the increase in the head width of the curved switch rail, the position of the maximum wear depth is transferred from the stock rail to the shoulder of the curved switch rail.

On the inner side of two rails, the gauge measurement point is 16 mm below the rail head. At the gauge measuring point, the curved switch rail's side wear values at each wear stage are calculated, as shown in Table 4. When the total passing weight is 10 Mt and 20 Mt, side wear only occurs on curved switch rails with head widths of 5 mm and 20 mm. No wear occurs at the gauge measuring point in the remaining positions.

When the total passing weight is 30 Mt, 40 Mt, and 50 Mt, the amount of side wear of the curved switch rail tends to increase first and then decrease. The side wear value of the curved switch rails reaches its maximum at a head width of 20 mm. As the widening of the head width, the wear decreases gradually. The maximum side wear of a curved switch rail with a head width of 20 mm is 5.3 mm when the total passing weight is 50 Mt.

Table 4. Side wear amount of curved switch rail with different wear stages (unit: mm).

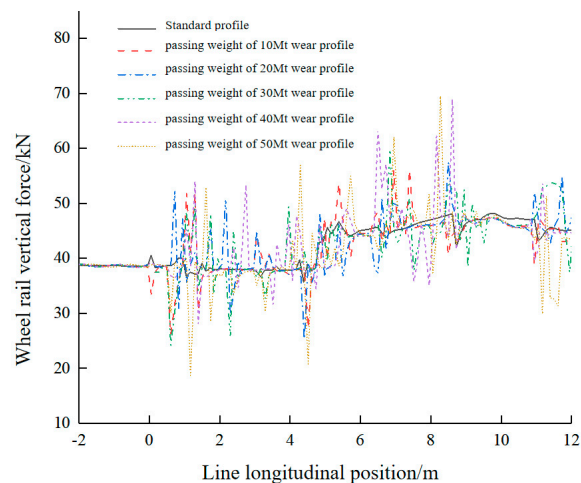
Head Width	Passing Weight				
	10 Mt	20 Mt	30 Mt	40 Mt	50 Mt
3 mm	0	0	0.10	0.64	1.18
5 mm	1.35	2.14	2.84	3.39	3.88
20 mm	0.99	2.23	3.30	4.28	5.30
35 mm	0	0	0.50	1.35	2.19
50 mm	0	0	0.07	0.64	1.24
72.2 mm	0	0	0.02	0.37	0.97

4. The Effect of Curved Switch Rail Wear on Vehicle Dynamic Performance

The next step is to investigate how curved switch rail wear affects vehicle dynamic performance as it passes through a curved switch rail from the perspective of stability and safety. The wheel with standard xp55 is selected to pass over the curved switch rails with standard and worn profiles. Five dynamic indices of the left wheel of the first wheelset, including wheel–rail vertical force, lateral force, derailment coefficient, and lateral and vertical acceleration, are studied when a vehicle passes over a curved switch rail at a speed of 80 km/h.

4.1. Vertical Force

Figure 9 depicts the variation trend of wheel–rail vertical force. The horizontal axis 0 point is defined as the tip of the curved switch rail. When the vehicle is driving in a straight line, the vertical force is about 38.65 kN. The change in vertical force is relatively stable when the vehicle travels on the standard profile curved switch rail.

**Figure 9.** Wheel–rail vertical forces of left wheel of the first wheelset.

When the vehicle travels to 4.83 m from the tip of the curved switch rail, the vertical force suddenly increases to 42.92 kN. When the vehicle is traveling on the non-worn curved switch rail, the vertical force fluctuation is small, and the range is 12.56 kN. The wheel–rail vertical force fluctuates to varying degrees when the vehicle is traveling on a worn curved switch rail. The range reaches a maximum of 50.72 kN, when the total weight of the vehicle is 50 Mt.

The maximum wheel–rail vertical forces when vehicles with different passing weights pass through the switch section are shown in Figure 10. The vertical force rises with the increase in the total passing weight, demonstrating a nonlinear positive correlation. When the total passing weight increases from 30 Mt to 40 Mt, the vertical force enhances significantly, which increases by 9.19 kN. The vertical force reaches a maximum value of 69.44 kN as the total passing weight reaches 50 Mt; compared with the standard wheel–rail

matching, it increased by 43.99%. The vertical force of all working conditions is less than the specified limit, meeting the safety regulations. The increase in vertical forces can cause the curved switch rail to be subjected to greater impacts, making it susceptible to craters and increasing the vertical vibration of vehicle travel.

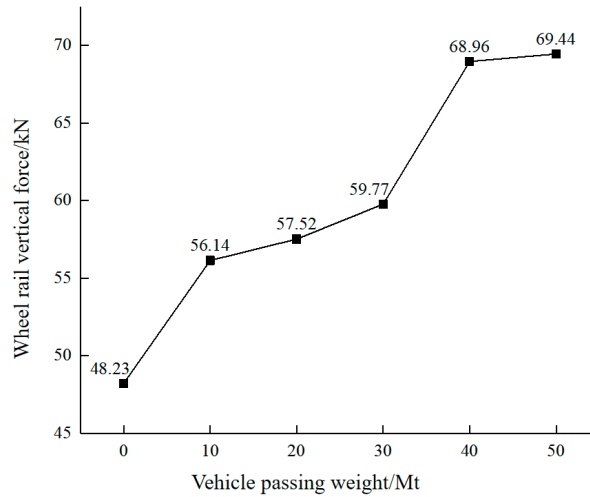


Figure 10. Comparison of the maximum value of wheel–rail vertical force.

4.2. Lateral Force

The variation trend of wheel–rail lateral force is shown in Figure 11. The direction of lateral force is specified as follows: the direction pointing to the inside of the rail is positive and the direction pointing to the outside of the rail is negative. At the initial stage when the vehicle enters the turnout, the lateral force is very small, only 445 N. When the vehicle travels from point 0 to 4.83 m, the lateral force suddenly increases to 20.86 kN.

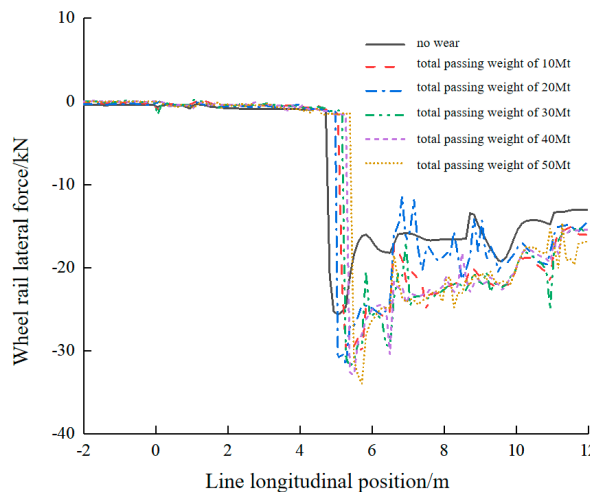


Figure 11. Wheel–rail lateral forces of left wheel of the first wheelset.

As the vehicle continues to travel, there is a certain decrease and accompanying fluctuation in the lateral force. The curved switch rail is a variable section structure where the lateral forces fluctuate due to changes in the wheel–rail contact state. The location of the abrupt lateral force change is slightly delayed after wear occurs on the curved switch rail. Compared with the standard wheel–rail interaction, the lateral force fluctuations are greater for wear rails. The range reaches a maximum of 20.35 kN when the total passing weight is 20 Mt.

The maximum wheel–rail vertical forces are shown in Figure 12. When the total passing weight increases from 10 Mt to 50 Mt, the lateral force rises from 25.66 kN to

33.95 kN. When the total passing weight reaches 50 Mt, the lateral force reaches a maximum value of 33.95 kN, which is a 32.33% increase compared to the maximum lateral force of 25.66 kN under standard wheel matching. The lateral force under the matching conditions of standard wheel and curved switch rail of different wear stages is less than the specified limitation, which meets the requirements of safety regulations. However, the increase in lateral force will increase the side wear of the curved switch rail, and then affect the wheel–rail contact state.

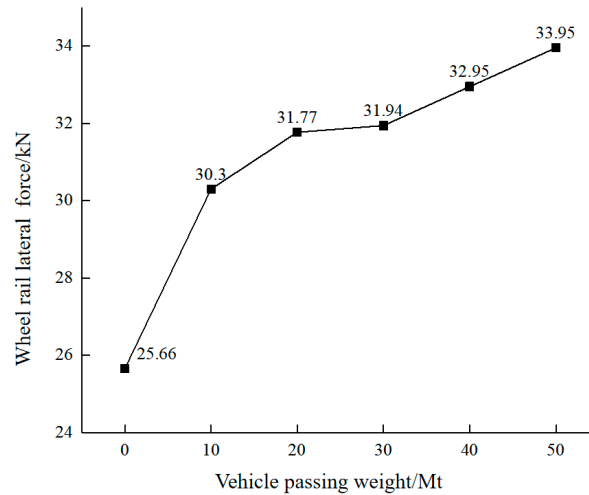


Figure 12. Comparison of the maximum value of wheel–rail lateral force.

4.3. Derailment Coefficient

Figure 13 shows that the derailment coefficient has a similar fluctuation trend. When the vehicle first enters the standard curved switch rail, the derailment coefficient is very small, only about 0.03. When the vehicle travels to 4.83 m from the 0 point, the derailment coefficient suddenly increases to 0.59. As the vehicle continues to travel, the derailment coefficient continues to fluctuate and decrease to a certain extent.

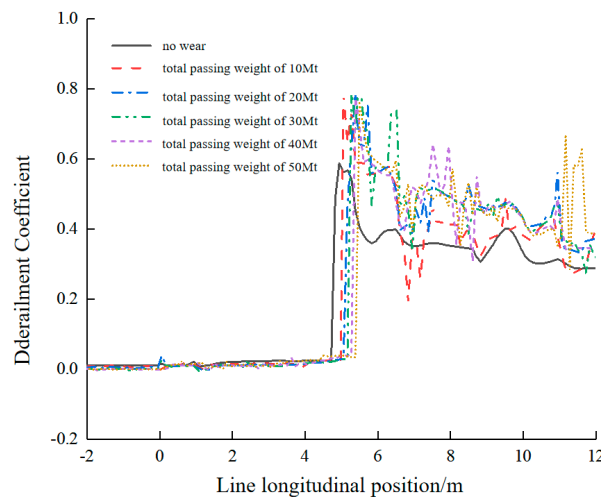


Figure 13. Wheel–rail derailment coefficient of left wheel of the first wheelset.

Figure 14 compares the maximum value of the wheel–rail derailment coefficient when the wheel passes the curved switch rail. The derailment coefficient tends to rise and then fall as the wear stage of the curved switch rail increases. When the total passing weight is 30 Mt, the derailment coefficient reaches the maximum of 0.79, which is 33.89% higher than the standard wheel–rail matching. At this time, it is close to the prescribed limitation and requires attention.

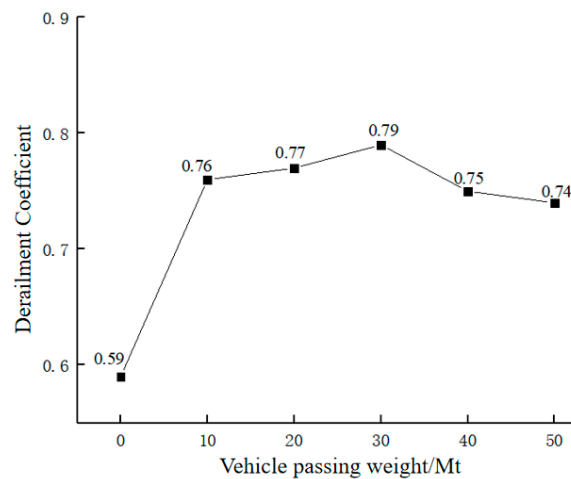


Figure 14. Comparison of the maximum value of wheel–rail derailment coefficient.

4.4. Vehicle Running Stability

Vehicle running stability reflects the comfort of passengers and the quality of vehicle operation. The vertical and lateral acceleration of the vehicle are the criteria for judging the stability of the vehicle. Figure 15a,b show the trends of vertical and lateral acceleration when the vehicle passes through curved switch rails with different wear stages, respectively.

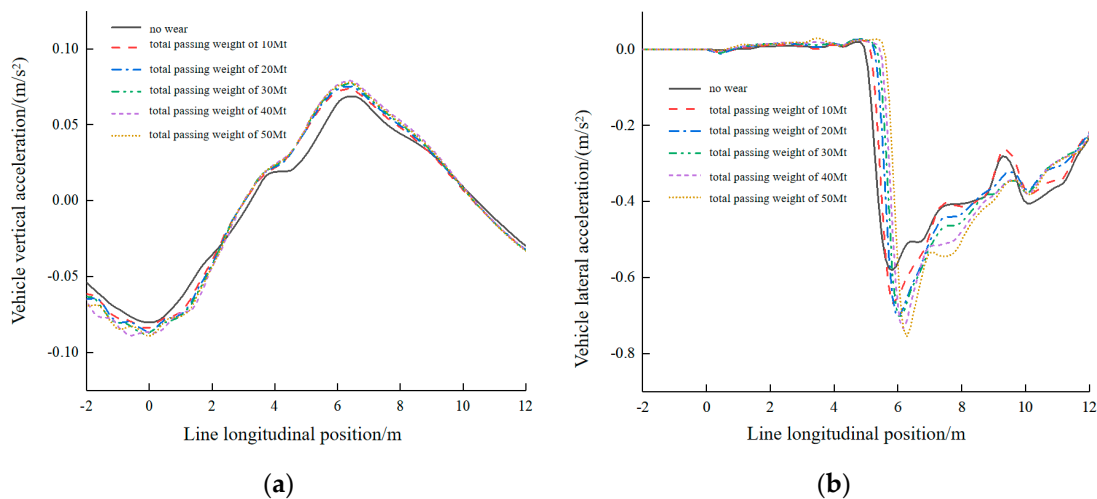


Figure 15. Vehicle acceleration under different worn curved switch rails: (a) vertical acceleration; (b) lateral acceleration.

The absolute maximum vertical acceleration ranged from 0.088~0.098 m/s^2 as the vehicle entered the vicinity of the 0 point. After completing the transition, the vertical acceleration continues to increase, with a maximum value between 0.08 and 0.089 m/s^2 . As a result of the transition between the wheels in these two positions, the vehicle will jump to a certain extent, increasing the vertical acceleration, and tends to decrease in the non–transition section. When the vehicle first enters the standard curved switch rail, the lateral acceleration is small, which is about 0.01 m/s^2 . When the vehicle travels to 5.83 m from the 0 point, the lateral acceleration increases to a maximum value of 0.58 m/s^2 . As the curved switch rail’s wear stage increases, the location of the sudden change in vehicle lateral acceleration gradually moves away from the 0 point.

The lateral acceleration rises with the increase in the total passing weight, and its maximum value is in the range of 0.58~0.76 m/s^2 . The lateral acceleration of the vehicle is 0.76 m/s^2 when the curved switch rail passes a total weight of 50 Mt. This is a 31.03% increase compared to the standard wheel–rail match. The vertical acceleration of the vehicle

increases with the total passing weight. When the total passing weight is 10 Mt, the vertical acceleration is 0.08 m/s^2 . The vertical acceleration reaches 0.089 m/s^2 , as the total passing weight is 50 Mt. It is 11.25% larger than the standard wheel–rail match. The wear of the curved switch rail has less effect on the vertical acceleration.

5. The Effect of Wheel Wear on Vehicle Dynamic Performance

The next step is to investigate how wheel wear affects a vehicle's dynamic performance as it passes over a curved switch rail from the perspective of stability and safety. The wheel with standard xp55 and different wear stages is selected to pass over the standard curved switch rail.

5.1. Vertical Force

The fluctuation trend of the wheel–rail vertical force is depicted in Figure 16. The wheel passing over the non-worn curved switch rail is similar at different stages of wear. Compared to the non-worn wheels, the worn wheel has greater vertical forces, and the fluctuation is large. The maximum range of vertical force when passing a turnout with a wear type IV wheel is 44.28 kN. The vertical force reaches the maximum at 8.17 m from the 0 point, which is 89.48 kN. Due to the wear of the wheel, the tread profile of the wheel has a certain depression near the nominal rolling circle. Wheel wear can lead to poor contact between the wheels and rails, intensifying the effect of vertical force between wheels and rails.

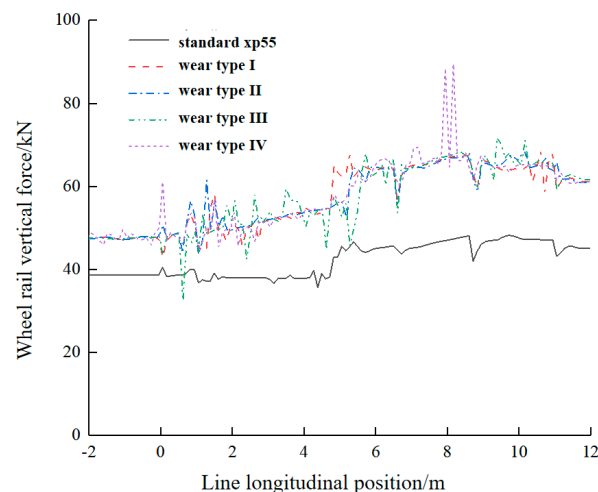


Figure 16. Wheel–rail vertical forces of left wheel of the first wheelset.

Figure 17 shows a comparison of the maximum vertical force values. The general trend of wheel–rail vertical force increases with increasing wheel wear. For wheels of wear types I, II, and III, the maximum vertical force through the curved switch rail is between 68.42 kN and 71.65 kN, with the three values being very close to each other. The maximum vertical force through the curved switch rail for the wheels of wear type IV is 89.48 kN, which is 85.53% more than that of the non-worn wheels. The calculated values of the wheel–rail force for the five conditions are less than the limit value of 170 kN, which is in line with the requirements of the safety regulations.

5.2. Lateral Force

The trend of the wheel–rail lateral force variation of the vehicle over the curved switch rail is similar for all types of wheels. Compared with non-worn wheels, the wheel–rail lateral forces are reduced when the wheels are worn. There is a certain delay in the complete transition of each wear wheel to the curved switch rail position, as shown in Figure 18. The wear type III wheel has the longest deferral distance for maximum wheel–rail lateral forces, reaching a maximum of 23.17 kN at 6.28 m from the tip of the curved switch rail.

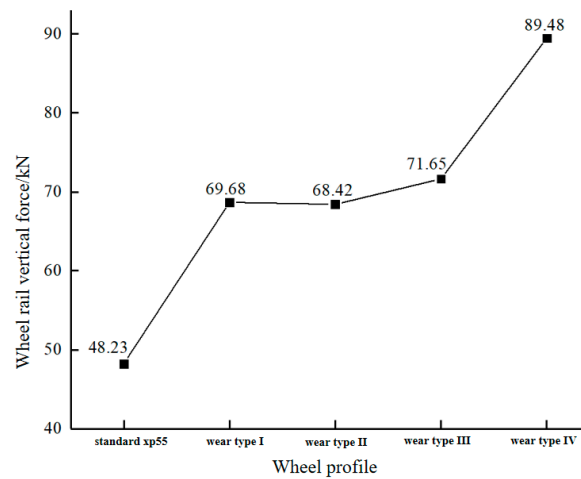


Figure 17. Comparison of the maximum value of wheel–rail vertical force.

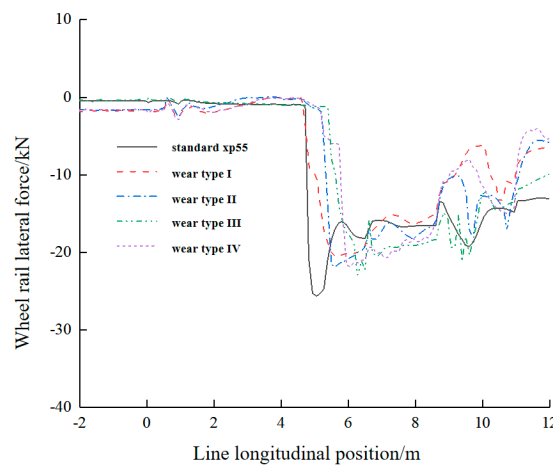


Figure 18. Wheel–rail lateral forces of left wheel of the first wheelset.

The following is a comparison of the lateral force’s maximum value (see Figure 19). It was found that the wear type I wheel passing over the curved switch rail had the minimum lateral force, which was 20.48 kN. The wear type III wheel has a lateral force of 23.17 kN, which is 13.13% higher than that of wear type I. The wheel–rail lateral force of the standard curved switch rail matched with wheels of different wear is less than the limit value of 48.4 kN.

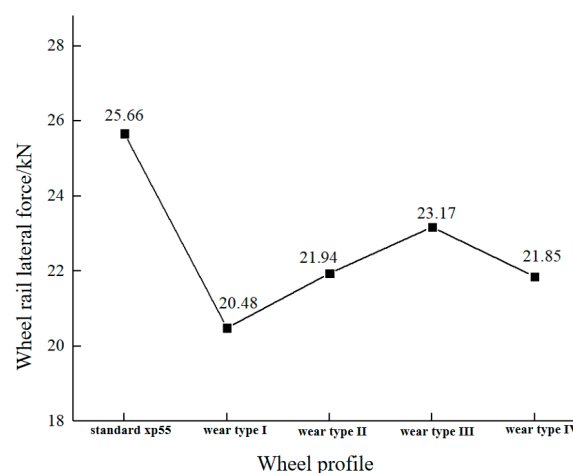


Figure 19. Comparison of the maximum value of wheel–rail lateral force.

5.3. Derailment Coefficient

The trends of the derailment coefficient are shown in Figure 20. The derailment coefficients of CRH5 vehicles with different wheels of wear stages passing over the non-worn curved switch rail are similar. Compared with the standard wheels, the derailment coefficient of the worn wheels is smaller. After the wheel runs in with the rail, the matching performance with the rail is improved. As the distance driven by the vehicle increases, the vehicle driving state gradually tends to stabilize, and the derailment coefficient progressively decreases after a sudden increase.

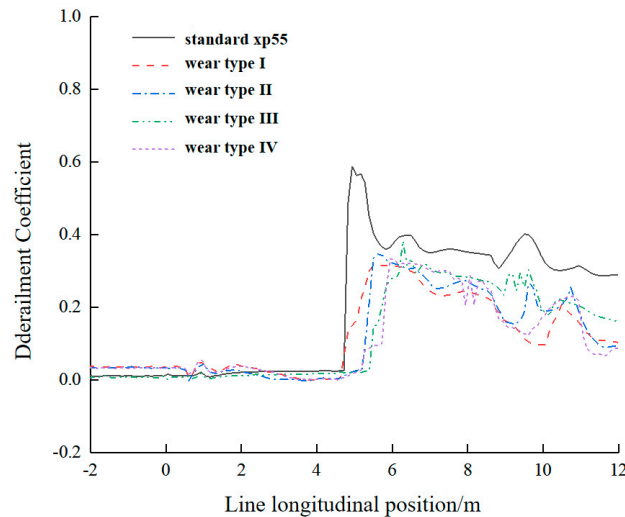


Figure 20. Wheel–rail derailment coefficient of left wheel of the first wheelset.

According to the comparison of the maximum value of derailment coefficient, when the wheel is not worn, the maximum value of the derailment coefficient is 0.59. As wheel wear occurs, the derailment coefficient tends to increase and then decrease with the increase in the wear stage. The smallest derailment coefficient is 0.32 under the action of the wear type I wheel. The derailment coefficient under the action of the wear type III wheel is the largest, which is 0.38. From Figure 21, it can be learned that the values of the derailment coefficient under each working condition are less than the specified limit value.

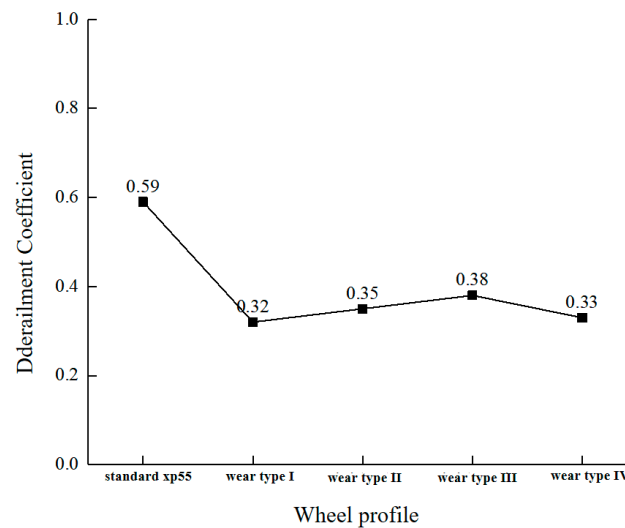


Figure 21. Comparison of the maximum value of wheel–rail derailment coefficient.

5.4. Vehicle Running Stability

Figure 22a,b show the trends of vertical and lateral acceleration, respectively. Each wear wheel traveling over the curved switch rail exhibits a similar trend and magnitude of vertical acceleration. As the stage when wheel wear increases, the vertical acceleration of the vehicle generally tends to increase, but the variation is small. The vertical acceleration increases from 1.421 to 1.444 m/s^2 , the range is only 0.023 m/s^2 . This means that as the wheel wear increases, the increase in wear has less of an effect on the vertical acceleration.

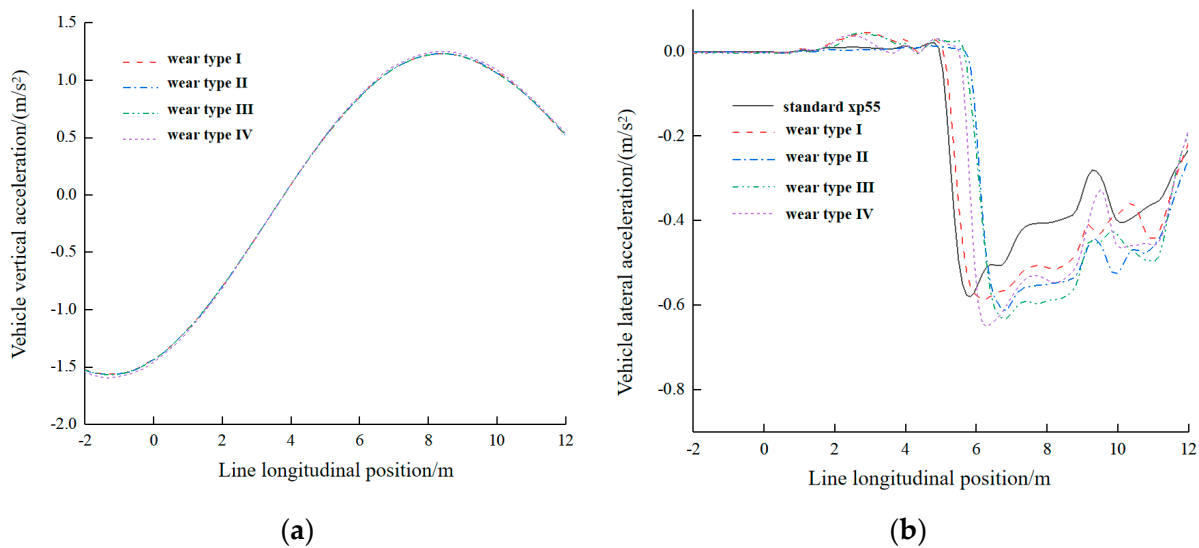


Figure 22. Vehicle acceleration under different worn wheels: (a) vertical acceleration; (b) lateral acceleration.

The lateral acceleration of a vehicle increases progressively as wheel wear rises, and the maximum value is between 0.58 and 0.65 m/s^2 . When a standard wheel passes through a non-worn curved switch rail, its maximum lateral acceleration is 0.58 m/s^2 . When a type IV wheel passes through a curved switch rail, the lateral acceleration reaches a maximum of 0.65 m/s^2 at a distance of 6.28 m from the 0 point, which is an increase of 12.07% compared with that of a non-worn wheel. The specified limit of lateral acceleration is 2.5 m/s^2 , and its maximum value for each working condition is much smaller than the limitation, which meets the safety standard.

6. Conclusions

A wear prediction model of the high-speed turnout curved switch rail is established in this study. The evolution law of the curved switch rail is analyzed using the wear prediction results. The effect of the wheel and rail wear on the dynamic performance of a vehicle passing through the curved switch rail in a high-speed turnout is investigated. The results show that:

- When the wheel passes through the area of the curved switch rail with a head width of 3–35 mm, the wheels make simultaneous contact with the stock rail and curved switch rail. As the head width increases, the height of the curved switch rail will exceed the height of the stock rail, and the wheels will travel from the stock rail to the curved switch rail. In the area with the head width of 35–50 mm, the wheel completely transitions to the curved switch rail.
- As the head width of the curved switch rail increases, the position of the maximum wear depth is transferred from the stock rail to the shoulder of the curved switch rail. For the same total passing weight, the side wear of the curved switch rail with a head width of 20 mm suffers the most severe wear. The cross-sectional area of the curved switch rail at the head width of 20 mm is small; the wheels transition from the stock

rail to the curved switch rail, and the wheel flange is close to the curved switch rail. This causes significant wear in this position.

- The wheel–rail vertical force, lateral force, and derailment coefficient all increase significantly when the vehicle wheels transfer from the stock rail to the curved switch rail. The wear of the wheels and rails has a higher impact on vehicle driving safety and a lower impact on vehicle driving stability.
- In all working conditions, when the standard wheel is matched with a curved switch rail with a total passing weight of 30 Mt, the maximum derailment coefficient reaches 0.79, which is close to the safety limit. It is recommended that for a curved switch rail with a total weight of 30 Mt, the frequency of detection and maintenance of the curved switch rail should be increased. The dynamic performance of the vehicle under other working conditions meets the prescribed limits of each dynamic index.

Author Contributions: Conceptualization, S.Y. and T.J.; methodology, J.Z.; software, S.Y. and T.J.; validation, S.Y. and T.J.; formal analysis, S.Y.; investigation, H.M. and Y.Z.; resources, J.Z.; data curation, S.Y. and H.M.; writing—original draft preparation, S.Y.; writing—review and editing, T.J., H.M. and Y.Z.; visualization, S.Y. and Y.Z.; supervision, J.Z.; project administration, J.Z.; funding acquisition, J.Z. and H.M. All authors have read and agreed to the published version of the manuscript.

Funding: This research was funded by the Natural Science Foundation of China (grant number 51775031) and the R&D Program of Beijing Municipal Education Commission (grant number KM202210016003).

Institutional Review Board Statement: Not applicable.

Informed Consent Statement: Not applicable.

Data Availability Statement: Not applicable.

Conflicts of Interest: The authors declare no conflict of interest.

References

1. Kassa, E.; Andersson, C.; Nielsen, O.C.J. Simulation of dynamic interaction between train and railway turnout. *Veh. Syst. Dyn.* **2006**, *44*, 247–258. [[CrossRef](#)]
2. Kassa, E.; Nielsen, O.C.J. Stochastic analysis of dynamic interaction between train and railway turnout. *Veh. Syst. Dyn.* **2008**, *46*, 429–449. [[CrossRef](#)]
3. Ma, X.C.; Wang, P.; Xu, J.M.; Chen, R. Comparison of non-Hertzian modeling approaches for wheel–rail rolling contact mechanics in the switch panel of a railway turnout. *Proc. Inst. Mech. Eng. Part F J. Rail Rapid Transit* **2019**, *233*, 466–476. [[CrossRef](#)]
4. Lu, W.J.; Tao, G.Q.; Wang, P.; Fu, Q.Y.; Guan, Q.H.; Wen, Z.F. Influence of Wheel Wear on Wheel–Rail Contact Behavior and Dynamic Performance of Metro Vehicle. *Eng. Mech.* **2017**, *34*, 222–231.
5. Yi, J.; Lei, P.C.; Cui, H.L.; Zhao, R.; Cui, D.B. Influence of hollow-worn wheels tread on running performance of EMU. *J. Railw. Sci. Eng.* **2020**, *17*, 297–305.
6. Sawley, K.; Urban, C.; Walker, R. The effect of hollow-worn wheels on vehicle stability in straight track. *Wear Int. J. Sci. Technol. Frict. Lubr. Wear* **2005**, *258*, 1100–1108. [[CrossRef](#)]
7. Sawley, K.; Wu, H. The formation of hollow-worn wheels and their effect on wheel/rail interaction. *Wear* **2004**, *258*, 1179–1186. [[CrossRef](#)]
8. Jin, X.S.; Zhao, G.T.; Liang, S.G.; Tao, G.Q.; Cui, D.B.; Wen, Z.F. Characteristics, Mechanisms, Influences and Counter Measures of High Speed Wheel/Rail Wear: Transverse Wear of Wheel Tread. *J. Mech. Eng.* **2018**, *54*, 3–13. [[CrossRef](#)]
9. Song, Y.; Du, Y.L.; Zhang, X.M.; Sun, B.C. Evaluating the Effect of Wheel Polygons on Dynamic Track Performance in High-Speed Railway Systems Using Co-Simulation Analysis. *Appl. Sci.* **2019**, *9*, 4165. [[CrossRef](#)]
10. Yang, Y.F.; Xu, M.K.; Ling, L.; Zhai, W.M. Polygonal wear evolution of locomotive wheels subjected to anti-slip control. *Wear* **2022**, *500–501*, 204348. [[CrossRef](#)]
11. Iwnicki, S.; Nielsen, J.C.O.; Gong, Q.T. Out-of-round railway wheels and polygonisation. *Veh. Syst. Dyn.* **2023**, *61*, 1785–1828. [[CrossRef](#)]
12. Wang, J.X.; Chen, X.; Li, X.G.; Wu, Y.J. Influence of heavy haul railway curve parameters on rail wear. *Eng. Fail. Anal.* **2015**, *57*, 511–520. [[CrossRef](#)]
13. Oliveira, L.A.M.D.; Kaewunruen, S.; Papaelias, M.; Li, T. A Novel Hybrid Method for Predicting Vertical Levelling Loss of Railway Track Geometry Under Dynamic Cyclic Loadings. *Int. J. Struct. Stab. Dyn.* **2022**, *22*, 2250162.
14. Li, T.; Su, Q.; Kaewunruen, S. Saturated Ground Vibration Analysis Based on a Three-Dimensional Coupled Train–Track–Soil Interaction Model. *Appl. Sci.* **2019**, *9*, 4991. [[CrossRef](#)]

15. Ridho, B.M.A.; Kaewunruen, S. Failure investigations into interspersed railway tracks exposed to flood and washaway conditions under moving train loads. *Eng. Fail. Anal.* **2021**, *129*, 105726. [[CrossRef](#)]
16. Hao, F.; Yushi, Y.; Sakdirat, K. Multi-Hazard Effects of Crosswinds on Cascading Failures of Conventional and Interspersed Railway Tracks Exposed to Ballast Washaway and Moving Train Loads. *Sensors* **2023**, *23*, 1786.
17. Kaewunruen, S.; Tang, T. Idealisations of Dynamic Modelling for Railway Ballast in Flood Conditions. *Appl. Sci.* **2019**, *9*, 1785. [[CrossRef](#)]
18. Pradhan, S.; Samantaray, A.K.; Bhattacharyya, R. Prediction of railway wheel wear and its influence on the vehicle dynamics in a specific operating sector of Indian railways network. *Wear* **2018**, *406*, 92–104. [[CrossRef](#)]
19. Wang, X.P.; Zhang, J.; Ma, H. Prediction Method of Wheel Wear of High Speed Train. *Tribology* **2018**, *38*, 462–467.
20. Wu, X.; Ding, J.J.; Qi, Z.; Wang, J.P.; Liu, L.Y. Study on the prediction of curve rail wear evolution and its influence on vehicle dynamics. *J. Railw. Sci. Eng.* **2020**, *17*, 460–468.
21. Ma, S.; Liu, X.B.; Re, S.B.; Chen, Z.; Liu, Y.T. Research on Side Wear Prediction of Curve Rail in Shuohuang Heavy Haul Railway. *J. Mech. Eng.* **2021**, *57*, 118–125.
22. Sun, Y.; Guo, Y.; Lv, K.K.; Chen, M.; Zhai, W.M. Effect of hollow-worn wheels on the evolution of rail wear. *Wear* **2019**, *436–437*, 203032. [[CrossRef](#)]
23. Sun, Y.; Guo, Y.; Zhai, W.M. Prediction of rail non-uniform wear—Influence of track random irregularity. *Wear* **2018**, *420–421*, 235–244. [[CrossRef](#)]
24. Li, S.Y.; Li, L.; Qi, Y.Y.; Li, J.; Mao, W.H. Rail Wear Prediction of Urban Rail Transit Line Curve Section. *Urban Mass Transit* **2023**, *26*, 57–61.
25. Gao, L.; Jiang, H.W.; Hou, B.W. Analysis on the Impact of No. 18 Fixed Frog with 60 and 60N Profiles on Turnout Crossing Dynamics and Wear. *China Railw.* **2021**, *60*, 15–21.
26. Wang, P.; Guo, Q. Study on the Effect of Wheel-rail Friction Control on Curved Switch Rail damage in Metro Turnout of China. *Transp. Rev.* **2020**, *42*, 72–77+82.
27. Wang, P.; Guo, Q.; Chen, J.Y. Research on the Effect of Wheel-rail Lubrication on Curved Switch Rail Wear in High-speed Turnout. *J. Railw. Eng. Soc.* **2019**, *36*, 17–22.
28. Zhang, W.R. Influence of Switch Rail Wear in Turnout on Train Running Safety. *Railw. Eng.* **2016**, *513*, 117–119+136.
29. Hamarat, M.; Papaalias, M.; Silvast, M.; Kaewunruen, S. The Effect of Unsupported Sleepers/Bearers on Dynamic Phenomena of a Railway Turnout System under Impact Loads. *Appl. Sci.* **2020**, *10*, 2320. [[CrossRef](#)]
30. Hamarat, M.; Kaewunruen, S.; Papaalias, M.; Silvast, M. New Insights from Multibody Dynamic Analyses of a Turnout System under Impact Loads. *Appl. Sci.* **2019**, *9*, 4080. [[CrossRef](#)]
31. Michele, M.; Astrid, P.; Nielsen, J.C.O.; Tore, V. Wheel–rail impact loads and axle bending stress simulated for generic distributions and shapes of discrete wheel tread damage. *J. Sound Vib.* **2021**, *502*, 116085.
32. Dindar, S.; Kaewunruen, S.; An, M. Bayesian network-based human error reliability assessment of derailments. *Reliab. Eng. Syst. Saf.* **2020**, *197*, 106825. [[CrossRef](#)]
33. Dindar, S.; Kaewunruen, S.; An, M. A hierarchical Bayesian-based model for hazard analysis of climate effect on failures of railway turnout components. *Reliab. Eng. Syst. Saf.* **2022**, *218*, 108130. [[CrossRef](#)]
34. Yang, Y.F.; Guo, X.R.; Ling, L.; Wang, K.Y.; Zhai, W.M. Effect of gauge corner lubrication on wheel/rail non-Hertzian contact and rail surface damage on the curves. *Acta Mech. Sin.* **2022**, *38*, 521522. [[CrossRef](#)]
35. Yang, Y.F.; Guo, X.R.; Sun, Y.; Ling, L.; Zhang, T.; Wang, K.Y.; Zhai, W.M. Non-Hertzian contact analysis of heavy-haul locomotive wheel/rail dynamic interactions under changeable friction conditions. *Veh. Syst. Dyn.* **2022**, *60*, 2167–2189. [[CrossRef](#)]
36. Carlberger, A.; Torstensson, T.P.; Nielsen, C.J.; Anders, F. An iterative methodology for the prediction of dynamic vehicle–track interaction and long-term periodic rail wear. *Proc. Inst. Mech. Eng. Part F J. Rail Rapid Transit* **2018**, *232*, 1718–1730. [[CrossRef](#)]
37. Piotrowski, J.; Chollet, H. Wheel–rail contact models for vehicle system dynamics including multi-point contact. *Veh. Syst. Dyn.* **2005**, *43*, 455–483. [[CrossRef](#)]
38. Piotrowski, J.; Kik, W. A simplified model of wheel/rail contact mechanics for non-Hertzian problems and its application in rail vehicle dynamic simulations. *Veh. Syst. Dyn.* **2008**, *46*, 27–48. [[CrossRef](#)]
39. Sh. Sichani, M.; Enblom, R.; Berg, M. A novel method to model wheel-rail normal contact in vehicle dynamics simulation. *Veh. Syst. Dyn.* **2014**, *52*, 1752–1764. [[CrossRef](#)]
40. Wang, P.; Zhou, J.Y.; Wang, P.J.; Chen, S.; An, B.Y. Comparative Study of Three Non-hertzian Rolling Contact Models. *J. China Railw. Soc.* **2022**, *44*, 39–47.
41. Ma, X.C.; Wang, P.; Xu, J.M.; Feng, Q.S. Analysis and Comparison of Different Wheel-rail Non-hertzian Rolling Contact Approaches in Railway Turnout. *J. Mech. Eng.* **2019**, *55*, 95–103.
42. Lin, F.T.; Weng, T.T.; Yang, Y.; Zhang, Z.H.; Jia, Z.; Chen, W.; Fang, Q.; Yang, J. Dynamic analysis of wear wheel in turnout frog area and influence of friction coefficient. *J. Railw. Sci. Eng.* **2023**, *20*, 1316–1325.
43. Fan, M.J.; Guan, Q.H.; Li, W.; Ma, W.G.; Wen, Z.F. Dynamic Response Analysis of Linear Motor Train Passing through the Branch Line of The Small Turnout. *Railw. Locomot. Car* **2021**, *41*, 70–76.
44. Wang, P. Experimental Study on Laws of Rail Wear Development of High Speed Turnout. *Railw. Eng.* **2019**, *59*, 109–112.
45. Wang, P. Prediction Analysis of Rail Wear in Switch Panel for No.42 High-Speed Turnout. *J. Southwest Jiaotong Univ.* **2021**, *56*, 289–299.

46. Schmid, R.; Endlicher, K.-O.; Lugner, P. Computer Simulation of the Dynamic Behavior of a Railway-Bogie Passing a Switch. *Veh. Syst. Dyn.* **1994**, *23*, 481–499. [[CrossRef](#)]
47. Archard, J.F. Contact and rubbing of flat surfaces. *J. Appl. Phys.* **1953**, *24*, 981–988. [[CrossRef](#)]
48. Jendel, T.; Berg, M. Prediction of Wheel Profile Wear. *Veh. Syst. Dyn.* **2002**, *37* (Suppl. S1), 502–513. [[CrossRef](#)]

Disclaimer/Publisher’s Note: The statements, opinions and data contained in all publications are solely those of the individual author(s) and contributor(s) and not of MDPI and/or the editor(s). MDPI and/or the editor(s) disclaim responsibility for any injury to people or property resulting from any ideas, methods, instructions or products referred to in the content.